INTERNATIONAL JOURNAL FOR NUMERICAL AND ANALYTICAL METHODS IN GEOMECHANICS, VOL. 16, 45–64 (1992)

PORE-PRESSURE RESPONSE DUE TO PENETRATION THROUGH LAYERED MEDIA

DEREK ELSWORTH

Department of Mineral Engineering, Pennsylvania State University, 104 Mineral Sciences Building, University Park, PA 16802, U.S.A.

SUMMARY

A solution is developed for a point dislocation traversing a slab of saturated porous material under prescribed upper and lower hydraulic boundary conditions as an analogue to penetration in a layer of finite thickness. Pressure response is conditioned by geometrical parameters and those of dimensionless penetration rate U_D, dimensionless time following penetration initiation t_D, and dimensionless time following penetration arrest t'_D. The extended set of dimensionless parameters controlling the response makes parameter determination problematic and questionably non-unique. Pressure response in the proximity of a lower permeable or impermeable boundary is indistinguishable from the homogeneous case for coefficients of consolidation c in excess of 2 cm^2/s. Below this threshold, penetration-generated pore pressures are visibly modified in the presence of a discrete boundary. *In situ* parameters inferred directly from pressure magnitudes, without due consideration for the influence of layering, may therefore be in considerable error. In the hydraulically visible range, the influence of layering on the generated tip pressures is apparent at a separation of the order of 1.5 cm for standard penetration. Although absolute pressure magnitudes are strongly modified in the presence of boundaries, dissipation rates remain relatively unaffected and are consistent with those recorded in the absence of boundaries. The monitoring of dissipation rates, post-arrest, is suggested as the most reliable and accurate method of extricating parameters, *in situ*.

1. INTRODUCTION

Piezocones have been successfully utilized in the determination of mechanical and hydraulic properties of soils, *in situ*.[1–4] Traditional methods of interpretation consider penetrometer advance or arrest to be conditioned by the homogeneous surrounding medium[5,6] without consideration of layering or lensing that may considerably affect the generation and subsequent dissipation of pore pressures. If the undrained strain field surrounding the penetrometer is determined, the pore-pressure distributions may be recovered from knowledge of the pore-pressure coefficients.[7,8] Alternatively, the analysis may be conducted using the concepts of deformation in a poro-elastic medium where pore-fluid pressures are conditioned by the induced deformation field.[9,10] Green's functions are available to represent both static[11] and moving[12] volumetric dislocations in poro–elastic media where the medium is homogeneous. Despite the inability of a linear analysis to represent the finite strain conditions likely at the tip of an advancing penetrometer, comparison with field data yields satisfactory agreement for penetration in unconsolidated media,[13] even when compared against approximate non-linear analyses.[14] This second-order influence of non-linearity appears conditioned by the essentially linear and small strain response of the material comprising the intermediate and far field. The applicability of a linear model may therefore diminish as the zone of non-linear behaviour surrounding the penetrometer becomes progressively larger. Additional application of dislocation models to

0363–9061/92/010045–20$10.00

Received 11 December 1990
Revised 14 June 1991

represent the complex coupled processes encountered in deep magmatic intrusion in saturated porous media[15] also appear successful. The excellent correspondence in matching field and model results suggests that the physical processes are adequately represented.

A method is proposed in the following to account for penetration in the presence of impermeable or constant pressure boundaries. Theory for a moving point dislocation in an infinite medium is extended where layer boundaries exert hydraulic resistance but enforce no specific stress or displacement conditions. Physically, this corresponds to a dislocation moving in the central horizontal layer of a three-layer system where all layers are of equivalent consolidation coefficient, but where permeabilities and moduli differ.

2. DISLOCATION THEORY

The equation for an instantaneous point normal dislocation introduced into an infinite saturated porous–elastic medium is given by Cleary[11] and for the specific case of a volumetric insertion of magnitude V,[12]

$$p - p^s = \frac{cV}{4\pi R^3}\frac{\mu}{k}\left(\frac{\xi^3}{2\sqrt{\pi}}e^{-\xi^2/4}\right) \tag{1}$$

where the magnitude of total fluid pressure p relative to the initial static pore pressure p^s is controlled by the coefficient of consolidation c of the saturated soil, permeability k, dynamic fluid viscosity μ and the radius of interest, R. The pressure field is spherically symmetric with the fluid dissipation process controlled through the dimensionless diffusion parameter ξ such that

$$\xi = \frac{R}{(ct)^{1/2}}; \quad R^2 = x^2 + y^2 + z^2 \tag{2}$$

with the Cartesian co-ordinate system (x, y, z) centred on the point dislocation and controlled by elapsed time since introduction, t.

The point normal dislocation of equation (1) may be readily integrated in time and space to represent the behaviour of a continuously moving or arrested dislocation,[12] where the fluid pressure and deformation field remains coupled, throughout. In this, the volumetric dislocation is the Green's function that reproduces displacement boundary conditions analogous to continuous insertion of a linear rod or penetrometer in an infinite medium. Pore-pressure generation and concurrent dissipation may be investigated in stratified media where discrete layers are bounded by materials of either much greater or much lower permeabilities. For practical purposes, where permeabilities in adjacent units differ by more than three or four orders of magnitude, the presence of the permeable or impermeable units may be represented by an enforced boundary condition. The zero-flux condition is used to represent a relatively impermeable bounding layer and the constant pressure condition for an adjoining permeable unit. These conditions may readily be enforced by use of distributed image dislocations or sources as investigated in the following.

2.1. *Moving dislocation*

The relationship for a moving point dislocation may be readily evaluated where the instantaneous dislocation volume V is replaced by a volumetric rate and integrated in time and space. For an amorphous penetrometer of radius r, introduced at constant velocity U, the substitution

$$V = U\pi r^2 \, d\tau \tag{3}$$

may be made with τ, the discrete parameter of time integration. A moving co-ordinate system is selected for the primary dislocation that moves with the dislocation at a rate U in the negative x-direction. The position of a point located relative to the primary dislocation at co-ordinates (x, y, z) at current time t would have been $[x - U(t - \tau), y, z]$ at time τ. Substituting equation (3) and the co-ordinate transformation into equation (1) and integrating over time (τ) between the time of initiation of penetration (0) and current time (t) gives[12]

$$P_D R_D = \frac{2}{\sqrt{\pi}} \int_{R_D/t_D^{1/2}}^{\infty} \exp\left[U_D x_D - \eta^2 - \left(\frac{U_D R_D}{2\eta} \right)^2 \right] d\eta \tag{4}$$

where the substitution $\eta = R/2[c(t - \tau)]^{1/2}$ is used as a dummy variable of integration and quantities are non-dimensionalised with respect to penetrometer radius, r. Thus,

$$P_D = \frac{4(p - p^s)}{Ur} \frac{k}{\mu} \tag{5}$$

$$U_D = \frac{Ur}{2c} \tag{6}$$

$$t_D = \frac{4ct}{r^2} \tag{7}$$

$$(x_D, y_D, z_D) = \frac{1}{r}(x, y, z) \tag{8}$$

with

$$R_D^2 = x_D^2 + y_D^2 + z_D^2 \tag{9}$$

where the terms may be referred to as dimensionless pressure P_D, dimensionless penetration rate U_D and dimensionless time t_D within the non-dimensional space (x_D, y_D, z_D). Dimensionless pressure is chosen specifically such that

$$0{\cdot}0 \leq P_D R_D \leq 1{\cdot}0 \tag{10}$$

for a single moving dislocation.

2.2 Image dislocations

Image dislocations must be supplied to enforce the boundary conditions mandated by the layered geometry represented in Figure 1. Penetration is initiated within a layer of thickness b at a height s above the lower layer boundary. The separation between any location in the moving co-ordinate x and the layer base is represented by w and $w = (s + x) - Ut$. Since the analysis is uncoupled, the image dislocations may also be viewed as fluid sources or sinks depending on the required boundary condition. Since the primary dislocation is reflected through a static confining boundary, as illustrated in Figure 1, the image dislocations must move at an identical rate (U) with the direction controlled by the reflection sequence of the confining stratigraphic boundaries. The disposition of image dislocations about the primary dislocation is given in Figure 2(a), where the first reflection is in the upper boundary, and in Figure 2(b), where the first reflection is in the lower boundary. These figures illustrate the initial primary co-ordinate system (x, y, z) and its derivatives (x_i', y_i', z_i') corresponding to time $t = 0$. Following the initiation of penetration, all local co-ordinate systems move at a rate U in the local negative x- or x_i'-direction as depicted in Figure 2. Penetration initiates in a layer of thickness b, at a height s above the layer base.

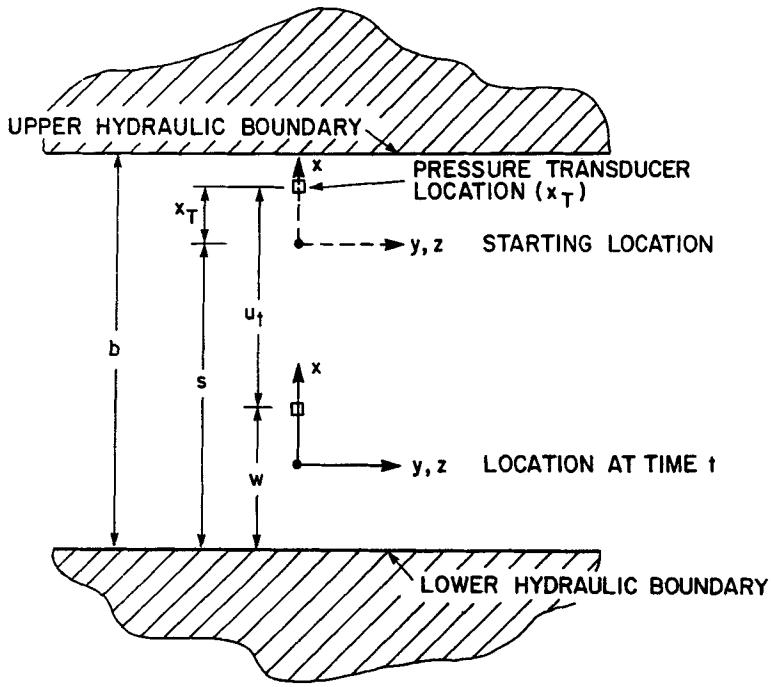

Figure 1. Layer geometry with moving co-ordinate system following the dislocation path

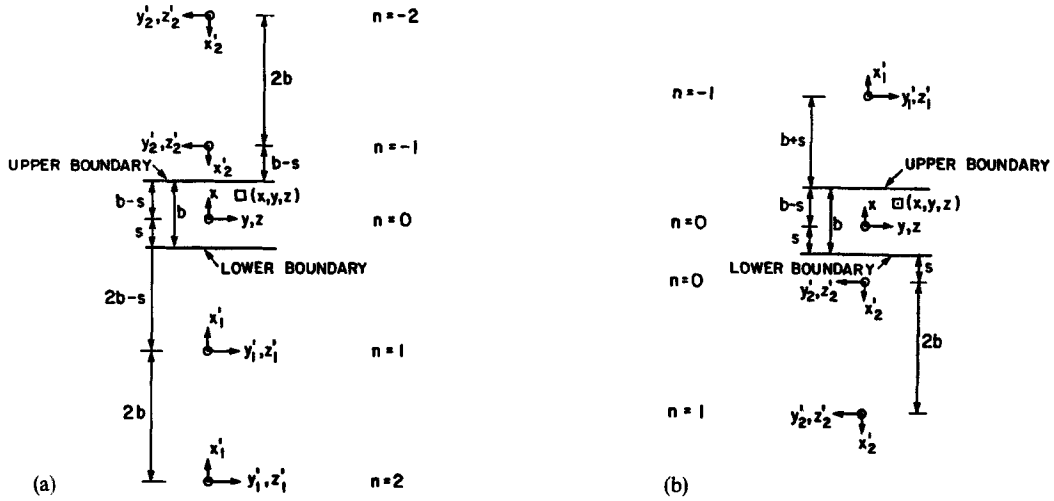

Figure 2. Image sources for central dislocation source ($n = 0$) illustrating numbering system and relative co-ordinates. First reflection about upper layer in (a) and about lower layer in (b)

The co-ordinates of any point in the moving (x, y, z) system of the primary source may be determined relative to the subsidiary (x_i', y_i', z_i') systems, where, from consideration of radial symmetry about the global x-axis, $y' = y$ and $z' = z$. Without reference to the sense of the image dislocations, transformed co-ordinates may be defined for the primary dislocation and the series

of images initiated following first reflection in the upper bounding layer [Figure 2(a)] as

$$x'_2 = -2(nb + s - Ut) - x, \quad n < 0 \tag{11a}$$

$$x'_1 = 2nb + x, \quad n \geq 0 \tag{11b}$$

A similar co-ordinate transformation may be applied to the sequence of images resulting from the first reflection in the lower bounding layer [Figure 2(b)] as

$$x'_1 = 2nb + x, \quad n < 0 \tag{12a}$$

$$x'_2 = -2(nb + s - Ut) - x, \quad n \geq 0 \tag{12b}$$

where the sense of the dislocation is controlled by the boundaries and

$$R'^2_{D_i} = \frac{1}{r^2}[x'^2_i + y'^2_i + z'^2_i] \tag{12c}$$

The relationships are symmetric despite the apparently antisymmetric appearance of equations (11) and (12).

This is true, not only with respect to the sequence of positive and negative source strengths with integer magnitude n, but also with respect to the relative orientations of global (x, y, z) and local (x'_i, y'_i, z'_i) co-ordinate systems.

Since all of the image co-ordinate systems move at a uniform velocity U in the local, negative x'_i-direction, a homogeneous expression is obtained by introducing, at the origin, a point dislocation at the rate $U\pi r^2$ per unit time. For the moving co-ordinate system, therefore, $V = U\pi r^2 \, d\tau$ and the integration is completed for relative co-ordinates

$$(x''_i, y''_i, z''_i) = [x'_i - U(t - \tau), y'_i, z'_i] \tag{13}$$

Substituting equations (11) and (12) into (13), rearranging in dimensionless form by dividing through by penetrometer radius, r, and substituting $\eta = R/2[c(t - \tau)]^{1/2}$ yields, for equations (11b) and (12a),

$$x''_{D_1} = 2nb_D + x_D - \frac{U_D R_D^2}{2\eta^2}, \quad -\infty < n < \infty \tag{14a}$$

and for equations (11a) and (12b),

$$x''_{D_2} = -2(nb_D - s_D) + U_D t_D - x_D - \frac{U_D R_D^2}{2\eta^2}, \quad -\infty < n < \infty \tag{14b}$$

where

$$b_D = \frac{b}{r}; \quad s_D = \frac{s}{r} \tag{14c}$$

and

$$y''_{D_i} = y_D; \quad z''_{D_i} = z_D \tag{14d}$$

Accordingly, equation (2) may be restated in dimensionless form as

$$\xi_i = \frac{R''_{D_i} r}{[c(t - \tau)]^{1/2}}; \quad R''^2_{D_i} = x''^2_{D_i} + y''^2_{D_i} + z''^2_{D_i} \tag{15}$$

and substituted into a modified form of equation (1) and integrated as

$$p - p^s = \sum_{i=1}^{2} \sum_{n=-\infty}^{\infty} \int_0^t \frac{cU\pi}{4\pi R_{D_i}''^3 r} \frac{\mu}{k} \left[\frac{\xi_i^3}{2\sqrt{\pi}} \exp\left(\frac{-\xi_i^2}{4} \right) \right] d\tau \tag{16}$$

When the substitution $\eta = R/2[c(t-\tau)]^{1/2}$ is made, the resulting integral becomes, following considerable re-arrangement,

$$P_D R_D = \frac{2}{\sqrt{\pi}} \sum_{n=-\infty}^{\infty} ij^n \int_{R_D/t_D^{1/2}}^{\infty} \exp\left\{ -\eta^2 \left[1 + a_1 \frac{(a_1 + 2x_D)}{R_D^2} \right] - \left(\frac{U_D R_D}{2\eta} \right)^2 + U_D(x_D + a_1) \right\} d\eta$$
$$+ \frac{2}{\sqrt{\pi}} \sum_{n=-\infty}^{\infty} lm^n \int_{R_D/t_D^{1/2}}^{\infty} \exp\left\{ -\eta^2 \left[1 + a_2 \frac{(a_2 - 2x_D)}{R_D^2} \right] - \left(\frac{U_D R_D}{2\eta} \right)^2 - U_D(x_D - a_2) \right\} d\eta \tag{17}$$

where

$$a_1 = 2nb_D \tag{18a}$$

$$a_2 = -2(nb_D + s_D - \tfrac{1}{2} U_D t_D) \tag{18b}$$

and i, j, l and m are all ± 1 depending on the stratigraphic sequencing. The image dislocations are positive in dilation and negative in contraction. Image dislocation sense is conditioned by the required upper and lower boundary conditions that sandwich the penetrated layer and are generalized in equation (17) where values of i, j l and m must be chosen accordingly. Physically, i and l control the sense of the primary and initial lower dislocations (i.e. for $n = 0$). Consequently, i is always positive and l is positive for an impermeable lower boundary and negative for a permeable one. The integers j and m regulate the asymmetry of the upper and lower boundary conditions with $j = m = +1$, then both upper and lower boundaries are impermeable or when both are permeable. When only one of the bounding layers is permeable then $j = m = -1$.

2.3. Penetration arrest

The instance of arrested penetration at time t' may be obtained most simply by superposing two concurrent sets of primary and image dislocations. The first set originates with penetration at $\tau = 0$ and runs at constant strength to the time of interest, $\tau = t$. A second set of dislocations of opposite sense begins at time $\tau = t'$ and runs at constant strength until $\tau = t$ for $t \geq t'$. The superposition results in a null effect for the dislocations introduced in the time $t' \leq \tau \leq t$. Although the pressure distribution is readily determined in this manner, the moving co-ordinate system translates a distance $U(t - t')$ in the period following arrrest. To determine the pressure distribution relative to the arrested geometry, the co-ordinate system must be translated in the x co-ordinate by substituting

$$x = \bar{x} + U(t - t'); \quad y = \bar{y}; \quad z = \bar{z} \tag{19}$$

or

$$x_D = \bar{x}_D + \tfrac{1}{2} U_D(t_D - t'_D); \quad y_D = \bar{y}_D; \quad z_D = \bar{z}_D \tag{20}$$

$$R_D^2 = \bar{R}_D^2 + U_D x_D(t_D - t'_D) + \tfrac{1}{4} U_D^2 (t_D - t'_D)^2 \tag{21}$$

$$t'_D = \frac{4ct'}{r^2} \tag{22}$$

where $(\bar{x}_D, \bar{y}_D, \bar{z}_D)$, and therefore, $\bar{R}_D$ are co-ordinates relative to the arrested geometry. Substituting equations (20)–(22) into (17), with revised integration limits, yields

$$P_D\bar{R}_D = \frac{\bar{R}_D}{R''_{D_1}}\frac{2}{\sqrt{\pi}}\sum_{n=-\infty}^{\infty} ij^n \int_{R_D/t_D^{1/2}}^{R_D/(t_D-t'_D)^{1/2}} \exp\left\{-\eta^2\left[1 + a_1\frac{(a_1+2x_D)}{R_D^2}\right] - \left[\frac{U_D R_D}{2\eta}\right]^2 + U_D(x_D + a_1)\right\} d\eta + \frac{\bar{R}_D}{R''_{D_2}}\frac{2}{\sqrt{\pi}}\sum_{n=-\infty}^{\infty} lm^n \int_{R_D/t_D^{1/2}}^{R_D/(t_D-t'_D)^{1/2}} \exp\left\{-\eta^2\left[1 + a_2\frac{(a_2-2x_D)}{R_D^2}\right] - \left[\frac{U_D R_D}{2\eta}\right]^2 - U_D(x_D - a_2)\right\} d\eta \quad (23)$$

where a_1 and a_2 are as previously defined in equation (18).

2.4. *Dimensionless parameters*

The pre-arrest and post-arrest pressure distributions represented by equations (17) and (23), respectively, may be reduced to a minimum set of dimensionless parameters. Pre-arrest, the functional dependence is

$$P_D R_D = f\left(U_D R_D; \frac{x_D}{R_D}; \frac{t_D}{R_D^2}; \frac{s_D}{R_D}; \frac{b_D}{s_D}\right) \quad (24)$$

and post-arrest this is modified to

$$P_D\bar{R}_D = f\left[U_D\bar{R}_D; \frac{\bar{x}_D}{R_D}; \frac{(t_D - t'_D)}{\bar{R}_D^2}; \frac{t'_D}{\bar{R}_D^2}; \frac{s_D}{R_D}; \frac{b_D}{s_D}\right] \quad (25)$$

where interest is retained in the local co-ordinate system relative to the arrested geometry.

The general form of the induced and concurrently dissipating pressure distribution around the moving dislocation is regulated in time by four groupings of dimensionless parameters and for the arrested case by five groupings. This multiplicity presents some problem for representation of the results in the form of type curves. The intractability is somewhat reduced if pressure distributions along the x-axis are only considered. Thus, $y_D = \bar{y}_D$, $z_D = \bar{z}_D = 0$ and $x_D/R_D = \bar{x}_D/\bar{R}_D = \pm 1$ and the number of dimensionless groups controlling the behaviour is reduced by one in both the pre-arrest and post-arrest modes.

3. SPECIALIZATIONS FOR SINGLE BOUNDARIES

Expressions developed for the most general case may be further specialized to represent simple problem geometries in an attempt to understand the interaction of the concurrent mechanisms controlling pressure generation and dissipation. In particular, the two specializations are for a dislocation approaching or leaving a hydraulic boundary.

3.1. *Single-boundary approach*

Where the dislocation approaches a single boundary, equations (17) and (23) may be modified by completing the summation for $n = 0$ only, and noting that $i = +1$ and $l = +1$ for an impermeable boundary and $l = -1$ for a permeable boundary. The pre-arrest condition may

then be stated as

$$P_D R_D = \frac{2}{\sqrt{\pi}} \int_{R_D/t_D^{1/2}}^{\infty} \exp\left[-\eta^2 - \left(\frac{U_D R_D}{2\eta}\right)^2 + U_D x_D \right] \left\{ 1 \pm \exp\left[(2x_D - a_2)\left(\frac{\eta^2 a_2}{R_D^2} - U_D\right)\right]\right\} d\eta \tag{26}$$

where $a_2 = -2s_D + U_D t_D$ and the positive and negative convention applies to the impermeable and permeable boundary conditons, respectively. It is important to note that the first exponential in equation (26) represents the behaviour of a moving dislocation in an infinite medium.[12]. The second bracketed term modifies the infinite medium response, returning an asymptotic magnitude of unity as $s_D \to \infty$, as might intuitively be expected.

Notably, equation (26) may be defined uniquely by the dimensionless groupings

$$P_D R_D = f\left(U_D R_D; \frac{x_D}{R_D}; \frac{t_D}{R_D^2}; \frac{s_D}{R_D} \right) \tag{27}$$

where, as expected, only a single additional parameter (s_D/R_D) is introduced over the variables controlling the infinite body response.

Dislocation arrest in the vicinity of a single boundary may be represented by simplifying equation (23) such that

$$P_D \bar{R}_D = \frac{\bar{R}_D}{R_D} \frac{2}{\sqrt{\pi}} \int_{R_D/t_D^{1/2}}^{R_D/(t_D - t'_D)^{1/2}} \exp\left[-\eta^2 - \left(\frac{U_D R_D}{2\eta}\right)^2 + U_D x_D \right] \left\{ 1 \pm \exp\left[(2x_D - a_2)\left(\frac{\eta^2 a_2}{R_D^2} - U_D\right)\right]\right\} d\eta \tag{28}$$

where the transformations of equations (20)–(22) apply and the controlling dimensionless groups are now expanded to

$$P_D \bar{R}_D = f\left[U_D \bar{R}_D; \frac{\bar{x}_D}{R_D}; \frac{(t_D - t'_D)}{\bar{R}_D^2}; \frac{t'_D}{\bar{R}_D^2}; \frac{s_D}{R_D} \right] \tag{29}$$

Significantly, the pore-pressure generation and dissipation behaviour in the presence of layer boundaries is modified through the second bracketed term in both equations (26) and (28). Since the image dislocations are of equal magnitude and either equal or of opposite sense, the integrated influence of the bracketed term must be bounded by zero and two. Two limiting cases are of signifiance. For a remote bounding layer,

$$S_D \to \infty \quad \text{and} \quad \exp\left[(2x_D - a_2)\left(\frac{\eta^2 a_2}{R_D^2} - U_D\right)\right] \to 0 \tag{30}$$

representing insignificant influence and where

$$x_D + s_D = \tfrac{1}{2} U_D t_D \quad \text{and} \quad \exp\left[(2x_D - a_2)\left(\frac{\eta^2 a_2}{R_D^2} - U_D\right)\right] \to 1 \tag{31}$$

corresponding to the pressure or pressure-gradient condition enforced at the layer boundary.

3.2. Single-boundary departure

A further specialization exists where a dislocation is initiated that moves downwards from an overlying boundary, where the lower hydraulic boundary is infinitely distant, or non-existent. The corresponding equations may be developed from equations (17) and (23), where the summation is restricted to $n = 0$ for the first term and $n = -1$ for the second term. The resulting expressions for the pre-arrest and post-arrest pressure distributions are identical to equations (26) and (28), respectively, where only the magnitude of a_2 differs. For single-boundary departure, a_2 may be specialized as

$$a_2 = 2(b_D - s_D) + U_D t_D \tag{32}$$

where $r(b_D - s_D)$ gives the location below the hydraulic boundary where penetration initiates. For a lower boundary at infinity, the chosen geometry of the system requires that $s_D \to \infty$ but, regardless, $(b_D - s_D)$ remains finite.

The dimensionless groups controlling behaviour of the system are, for the pre-arrest situation,

$$P_D \bar{R}_D = f\left[U_D R_D; \frac{x_D}{R_D}; \frac{t_D}{R_D^2}; \frac{(b_D - s_D)}{R_D} \right] \tag{33}$$

and for the post-arrest condition,

$$P_D \bar{R}_D = f\left[U_D \bar{R}_D; \frac{\bar{x}_D}{\bar{R}_D}; \frac{(t_D - t'_D)}{\bar{R}_D^2}; \frac{t_D}{\bar{R}_D^2}; \frac{(b_D - s_D)}{\bar{R}_D} \right] \tag{34}$$

Similar to the behaviour of a dislocation approaching a hydraulic boundary, the infinite homogeneous body solution is modified through the second bracketed terms of equations (26) and (28). The significant limiting cases are, for a remote upper bounding layer,

$$(b_D - s_D) \to \infty \quad \text{and} \quad \exp\left[(2x_D - a_2)\left(\frac{\eta^2 a_2}{R_D^2} - U_D \right) \right] \to 0 \tag{35}$$

representing insignificant modification of the infinite homogeneous body problem, and where

$$x_D - (b_D - s_D) = \tfrac{1}{2} U_D t_D \quad \text{and} \quad \exp\left[(2x_D - a_2)\left(\frac{\eta^2 a_2}{R_D^2} - U_D \right) \right] \to 1 \tag{36}$$

confirming that the boundary conditions at $x = (b - s) - Ut$, corresponding to the upper hydraulic boundary, are correctly and continuously enforced.

4. PORE-PRESSURE GENERATION

The magnitudes of pore pressures generated as a dislocation approaches an underlying hydraulic boundary may be used as an analogue to piezocone penetration in the presence of layering. Since piezocone pressures are normally recorded with depth, it is convenient to restate dimensionless time t_D in terms of a height ($w_D = w/r$) above the interface. Since, from Figure 1, $w = s + x - Ut$,

$$t_D = \frac{2}{U_D}(s_D + x_D - w_D) \tag{37}$$

and the appropriate dimensionless groupings are therefore

$$P_D R_D = f\left(U_D R_D; \frac{x_D}{R_D}; \frac{w_D}{R_D}; \frac{s_D}{R_D}; \frac{b_D}{R_D} \right) \tag{38}$$

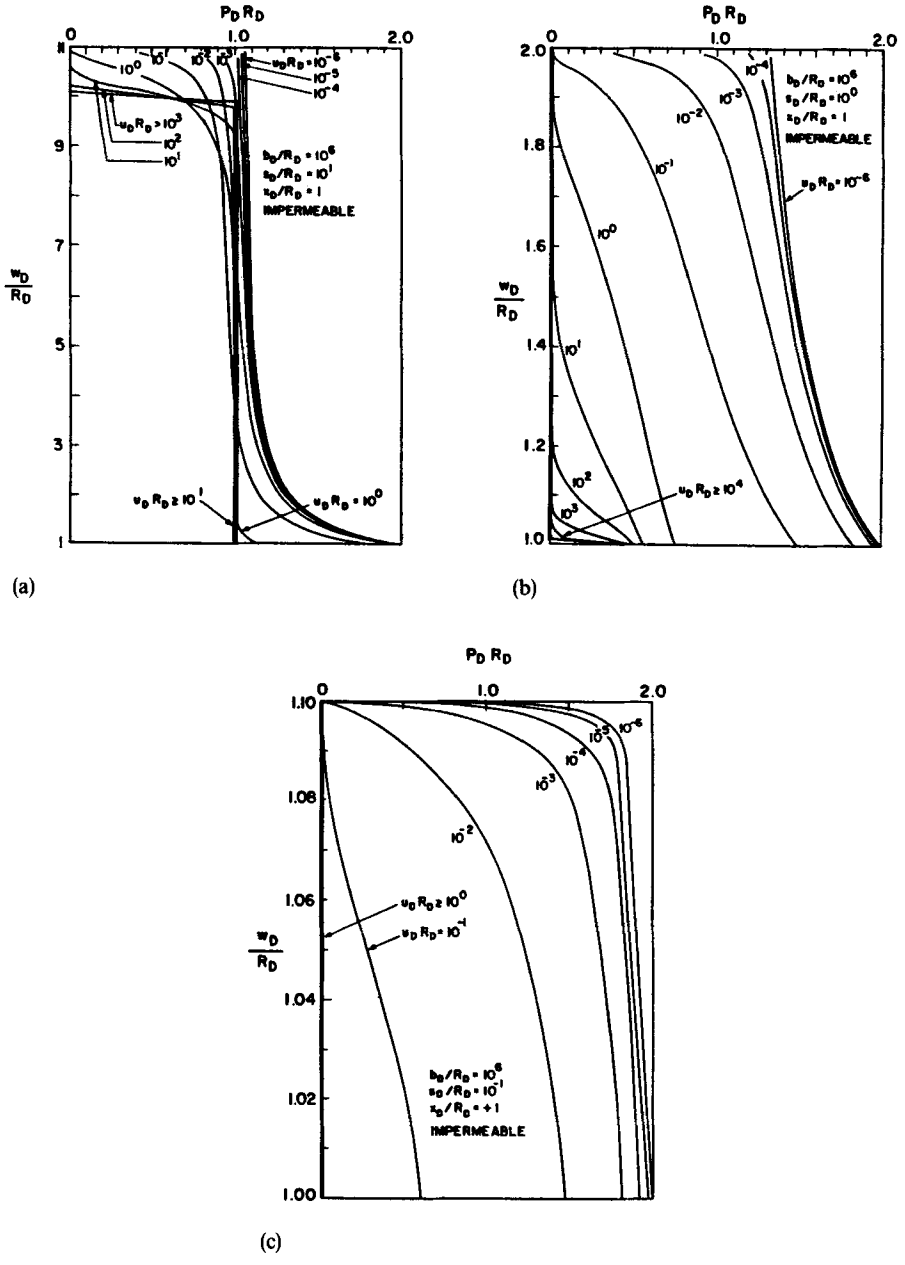

Figure 3. Pressure-generation profiles on the x-axis (shaft) for a dislocation approaching an impermeable lower boundary for (a) $s_D/R_D = 10^1$, (b) $s_D/R_D = 10^0$ and (c) $s_D/R_D = 10^{-1}$

allowing pressure behaviour to be evaluated for a wide range of penetration rate magnitudes. Responses for penetration within a thick layer ($b_D/R_D = 10^6$) are illustrated in Figures 3–6.

Figures 3(a)–3(c) illustrate dimensionless shaft-pressure generation profiles for penetration initiating at dimensionless heights of $s_D/R_D = 10^1$, 10^0, and 10^{-1} above the lower impermeable

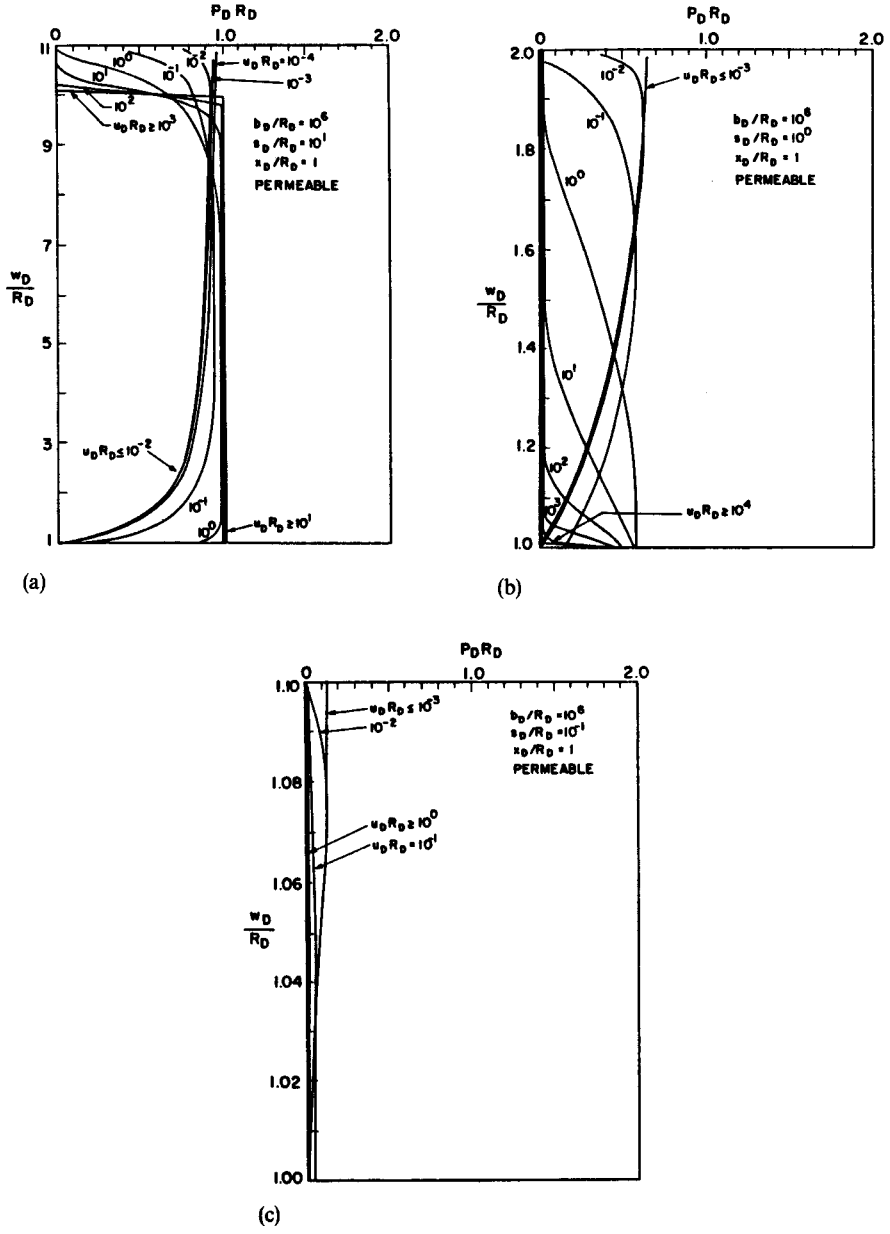

Figure 4. Pressure-generation profiles on the x-axis (shaft) for a dislocation approaching a permeable lower boundary for (a) $s_D/R_D = 10^1$, (b) $s_D/R_D = 10^0$ and (c) $s_D/R_D = 10^{-1}$

boundary. The development of pore pressures are most rapid for small magnitudes of dimensionless penetration rate, corresponding to low penetration velocities or their corollary of high magnitude of consolidation coefficient, c. Little influence of the boundary is seen as it is approached by the dislocation at high rate [$U_D R_D \geq 10^1$ in Figure 3(a)] or conversely, where the coefficient of consolidation is sufficiently low that pressure generation has not yet sufficiently

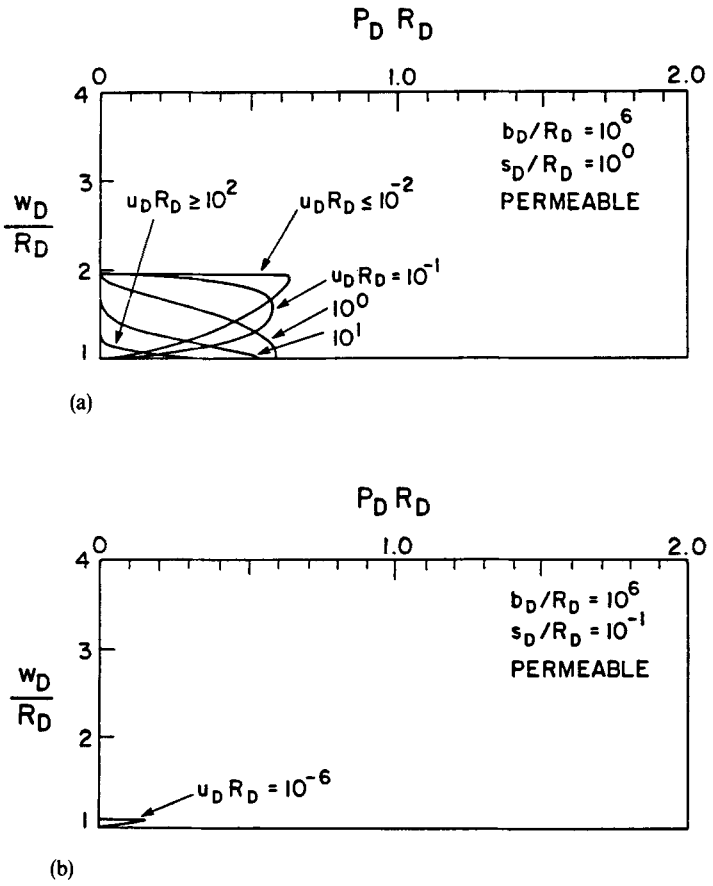

Figure 5. Pressure-generation profiles on the x-axis (shaft) for a dislocation approaching a permeable lower boundary for (a) $s_D/R_D = 10^0$ and (b) $s_D/R_D = 10^{-1}$ where height scales are equivalent

developed. The presence of the impermeable boundary is usually evidenced by an upturn in the concavity of the pressure profile with depth as apparent in Figures 3(b) and 3(c). For the increasingly shorter penetration lengths illustrated in Figures 3(b) and 3(c), the opportunity for the steady, pore-pressure conditions to develop is successively curtailed. Thus, a null-pressure response for $U_D R_D \geq 10^0$ is returned for $s_D/R_D = 10^{-1}$ whereas for larger s_D/R_D the full steady condition is reached. Significantly, the influence of an impermeable boundary is felt earlier (in space) where the real penetration rate decreases or the coefficient of consolidation increases. The visibility of an impermeable layer appears to be limited to the range $w_D/R_D \leq 2$, for media with the highest consolidation coefficient, corresponding to a location equally far ahead of the advancing dislocation as the monitoring location is behind. A further characteristic of note is that for $U_D R_D \geq 10^1$, the presence of the impermeable boundary is not evident in the response of Figures 3(a)–3(c). Physically, this corresponds to the penetrated medium having a sufficiently slow pressure response (in turn a direct consequence of a low c-magnitude) that the presence of a boundary is effectively masked.

The responses for a dislocation approaching a permeable boundary for an identical spread of parameters ($b_D/R_D = 10^6$; $s_D/R_D = 10^1$; 10^0; 10^{-1}) are illustrated in Figures 4 and 5. Pressure

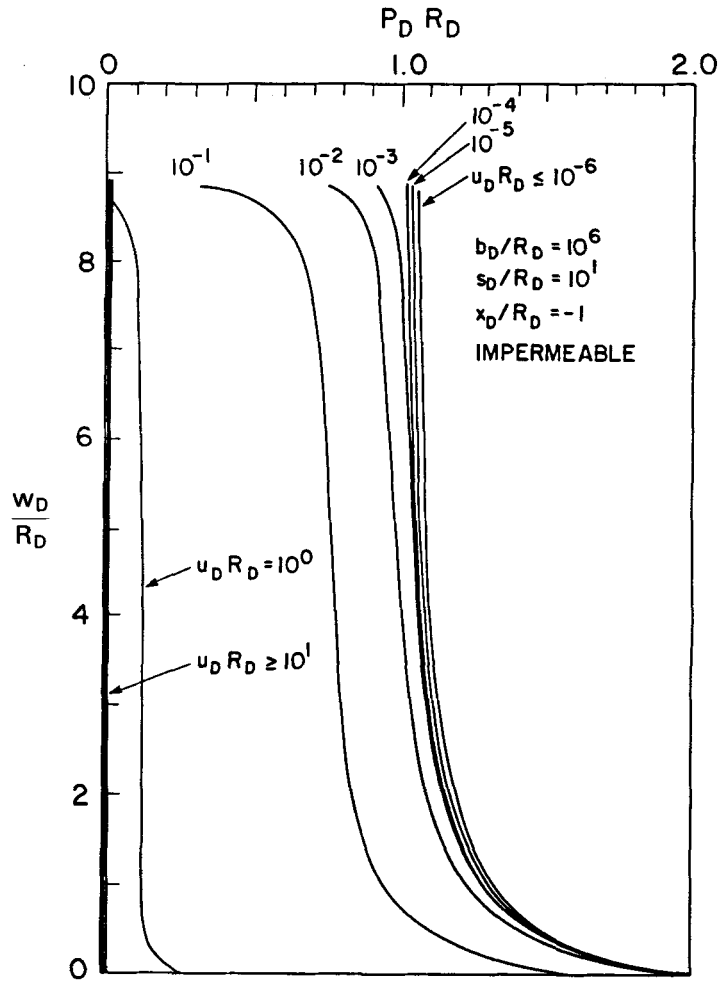

Figure 6. Pressure-generation profiles on the negative x-axis (tip) for a dislocation approaching an impermeable lower boundary for $s_D/R_D = 10^1$

generation is similar for large heights of penetration initiation ($s_D/R_D = 10^1$) but is curtailed as the permeable or constant pressure boundary becomes closer to the start-up location. The pressure response close to the boundary is of opposite sense to that for an impermeable interface with the presence of an interface being felt within the range $w_D/R_D \leq 2$. Again, the greatest influence is apparent for small magnitudes of U_D corresponding to large magnitudes of consolidation coefficient with response being blind to the feature for $U_D R_D \geq 10^1$. Where the depth scales of Figures 4(b) and 4(c) are compressed to a common magnitude in Figures 5(a) and 5(b), the characteristic forms of erratic pore-pressure magnitudes common to piezocone records in layered media are replicated.

Where the dislocation method is used as an analogue to cone penetration, a centre of volume expansion concept[13] has been proposed such that the tip for a standard 60 degree cone would be present at $x_D = -0{\cdot}4082$. Pressure response for a cone approaching an impermeable boundary is illustrated in Figure 6 for $x_D/R_D = -1$ and $s_D/R_D = 10^1$. Only for penetration rate magnitudes

$U_D R_D \leq 10^0$ is the presence of the layer discernable. For tip pressures measured under standard penetration at 2 cm/s, a $U_D R_D$ of 10^0 corresponds to $c = 0{\cdot}72\ \text{cm}^2/\text{s}$. Thus, the presence of impermeable boundaries may be felt for media exhibiting c-magnitudes greater than this where the detection length is of the order $w_D/R_D \leq 2$ or approximately 1·5 cm ahead of the tip. Similar thresholds are evident for a penetrometer approaching a constant pressure boundary, where merely the sense of the pressure change with depth is altered.

5. PORE-PRESSURE DISSIPATION

In addition to influencing the pore-pressure magnitudes generated through penetration, the presence of conductive or impermeable boundaries may also influence the dissipation behaviour, post-arrest. The additional parameter w'_D is adopted corresponding to the height above the lower boundary at which penetration is arrested. Accordingly, the time of arrest $t'_D/\bar{R}_D^2$ is obtained from equation (37) as

$$\frac{t'_D}{\bar{R}_D^2} = \frac{2}{U_D \bar{R}_D}\left[\frac{s_D}{\bar{R}_D} + \frac{x_D}{\bar{R}_D} - \frac{w'_D}{\bar{R}_D}\right] \tag{39}$$

to provide the definitive grouping of dimensionless parameters as

$$P_D \bar{R}_D = f\left[U_D \bar{R}_D; \frac{x_D}{\bar{R}_D}; \frac{w'_D}{\bar{R}_D}; \frac{s_D}{\bar{R}_D}; \frac{(t_D - t'_D)}{\bar{R}_D^2}\right] \tag{40}$$

Pressure-dissipation profiles for shaft pressures elicited from a dislocation arrested close to an impermeable boundary are illustrated in Figures 7(a)–7(c). The ratio $w'_D/\bar{R}_D = 1$ represents arrest at the boundary, and $w_D/R_D > 1$ arrest prior to reaching the boundary. The pre-arrest steady pressures are those evident in Figure 3(a). Similar to the generation of pore pressures examined earlier, the influence of the boundary is not evident for $U_D \bar{R}_D \geq 10^1$, where both the magnitude of the steady pressure ($P_D \bar{R}_D$) and the dissipation behaviour differ insignificantly from those of an infinite homogeneous medium. As $U_D \bar{R}_D$ increases, the steady pressures approach the maximum attainable magnitude (for $b_D/R_D = 10^6$) of 2. Although the presence of a boundary has a considerable influence on the generated magnitude of pore pressures, dissipation rates remain virtually unchanged over the homogeneous instance for measurement locations on the shaft. The influence of a boundary is greatest for $w'_D/\bar{R}_D = 10^0$ in Figure 7(a) and diminishes for the successive magnitudes of $w'_D/\bar{R}_D = 3 \times 10^0$ and 10^1 represented in the responses of Figures 7(b) and 7(c), respectively. Response rates, however, remain fixed in dimensionless time with only the initial, pre-arrest pressure magnitude modifying the results. For $w'_D/\bar{R}_D \geq 10^1$, the response is ostensibly indistinguishable from that of a homogeneous body.

For standard penetration at rate $U = 2$ cm/s, $U_D = 10^0$ corresponds to $c = 1{\cdot}78\ \text{cm}^2/\text{s}$ and, therefore, the most interesting set of dissipation curves are for $U_D \bar{R}_D \leq 10^{-1}$ corresponding to penetration in materials of compressibilities comparable to silts or stiffer. Apparent from Figures 7(a)–7(c) is that both shaft pressures and dissipation rates remain relatively unaffected by the presence of boundaries in these materials.

Where the dislocation is arrested proximal to a constant pressure boundary, the responses are illustrated in Figures 8(a)–8(c). The response differs most from the behaviour of a homogeneous body, where the dislocation contacts the permeable layer for $w_D/\bar{R}_D = 10^0$ in Figure 8(a). Steady pressures are modified by the presence of the boundary only for $U_D \bar{R}_D \leq 10^0$. The consequence of this is that dissipation records may be lost where $U_D \bar{R}_D \leq 10^0$, corresponding to more permeable media (high c), where hydraulic communication is rapid. As anticipated, this effect is

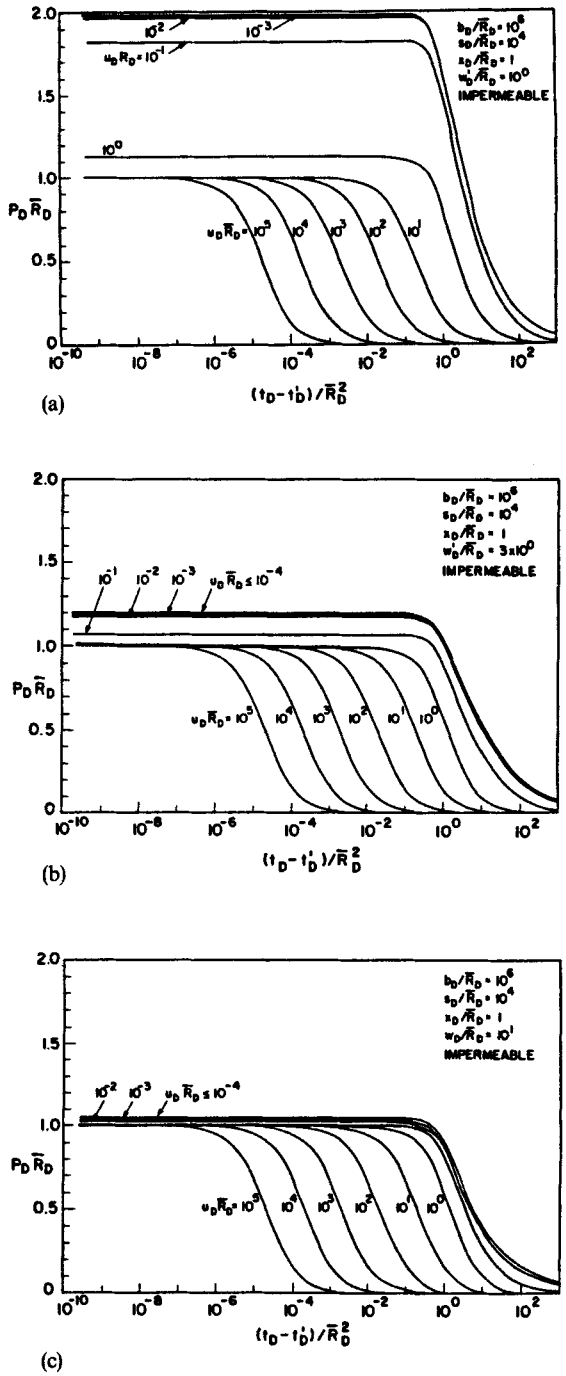

Figure 7. Pressure dissipation on positive x-axis (shaft) close to an impermeable boundary at heights (a) $w'_D/\bar{R}_D = 10^0$, (b) $w'_D/\bar{R}_D = 3 \times 10^0$ and (c) $w'_D/\bar{R}_D = 10^1$

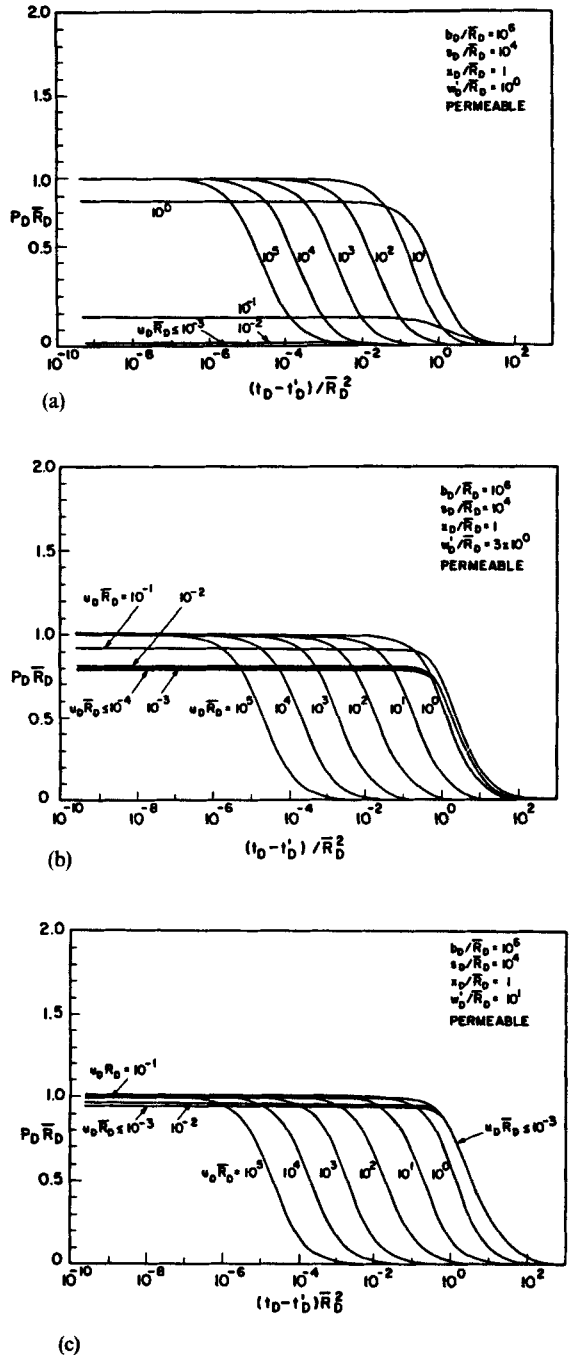

Figure 8. Pressure dissipation on positive x-axis (shaft) close to a permeable boundary at heights (a) $w'_D/\bar{R}_D = 10^0$, (b) $w'_D/\bar{R}_D = 3 \times 10^0$ and (c) $w'_D/\bar{R}_D = 10^1$

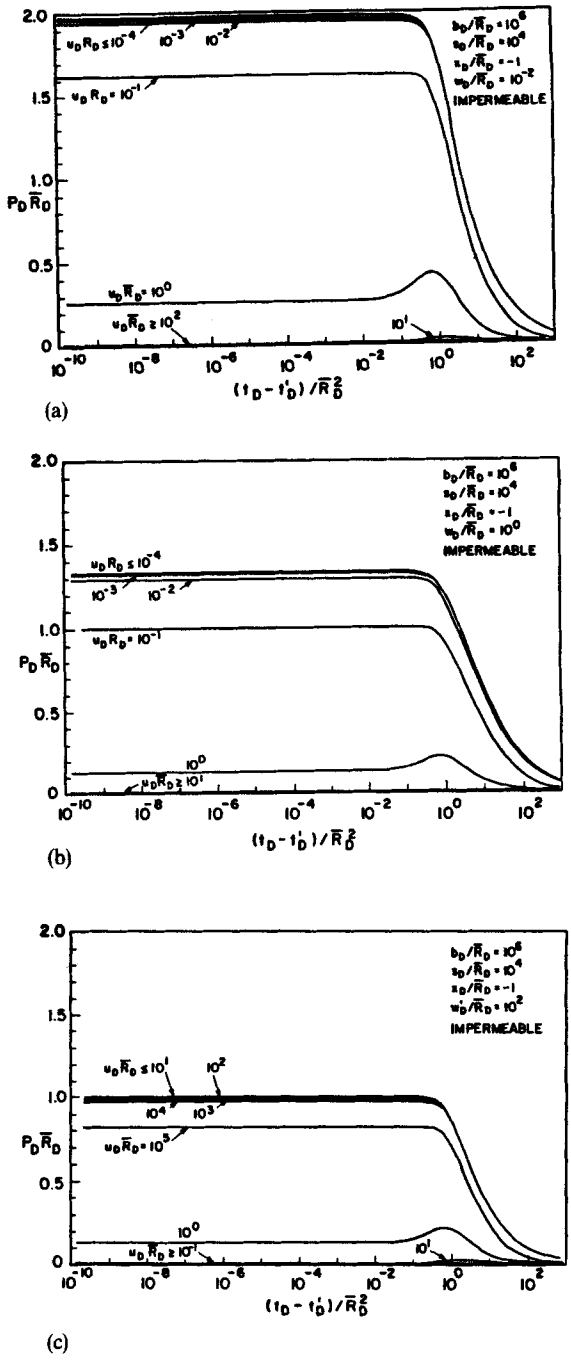

Figure 9. Pressure dissipation on negative x-axis (tip) close to an impermeable boundary at heights (a) $w'_D/\bar{R}_D = 10^0$, (b) $w'_D/\bar{R}_D = 3 \times 10^0$ and (c) $w'_D/\bar{R}_D = 10^1$

most acute where penetration is arrested on the hydraulic boundary. As penetration is arrested successively higher, as illustrated in Figures 8(b) and 8(c) for $w'_D/\bar{R}_D = 3 \times 10^0$, and 10^1 respectively, the influence diminishes. Again, dissipation rates are not significantly influenced by the presence of a boundary.

Dissipation records for a penetrometer tip ($x_D/R_D = -1$) are illustrated in Figures 9(a)–9(c) for separations from an impermeable bounding layer of $w'_D/\bar{R}_D = 10^{-2}, 10^0, 10^2$. The influence of the bounding layer is greatest for $w'_D/\bar{R}_D = 10^{-2}$, where dimensionless pressures for $U_D\bar{R}_D \leq 10^{-2}$ approach the upper threshold of 2·0. For low-compressibility media ($U_D\bar{R}_D \geq 10^2$) the steady pressure generation magnitude is extremely small but increases in the vicinity of the tip following arrest.

For tip pressures, dissipation rates are considerably more homogeneous in dimensionless time than for those measured on the shaft. Significantly, the influence of a hydraulic boundary is shown to have negligible influence on the dissipation rate at the tip as is evident from Figures 9(a)–9(c). This suggests that time for fifty per cent dissipation should remain a reliable parameter in the evaluation of c from tip pore-pressure records.

Where the penetrometer tip approaches a constant pressure boundary, the magnitude is decreased as $w'_D/\bar{R}_D$ approaches zero. Where $w'_D/\bar{R}_D > 10^2$, the influence of the boundary is not apparent and the steady pressures approach those for a homogeneous medium. Although absolute pressure magnitudes are considerably reduced as $w'_D/\bar{R}_D$ is decreased, the dissipation process appears relatively unaffected over a broad range of arrest heights w'_D. This is particularly significant since, for a standard penetrometer, $w'_D/\bar{R}_D = 10^{-2}, 10^0, 10^2$ correspond to the presence of boundaries within $w = 0{\cdot}73 \times 10^{-2}$, 0·75 and $0{\cdot}75 \times 10^2$ cm of the penetrometer tip.

6. CONCLUSIONS

The powerful analogy established between a moving point dislocation and penetrometer advance in a saturated porous solid allows pre- and post-arrest pore-pressure distributions to be determined in layered media. Comparisons are drawn to infer the influence of impermeable or permeable boundaries on the resulting pressure response and provide quantitative evaluation of the reliability and accuracy of parameter estimates based on the assumption of a homogeneous medium. The important conclusions are as follows:

1. The steady shaft-pressure distribution ($x_D/R_D = +1$) in an infinite homogeneous medium is given by $P_D R_D = 1{\cdot}0$. This is modified in the presence of a single boundary as $0{\cdot}0 \leq P_D R_D \leq 2{\cdot}0$ depending on the boundary type. For layers of finite thickness, the upper limit of dimensionless pressure is undefined. Since this variation in dimensionless pressure magnitude is apparent when both the dislocation and the monitoring location are confined within a layer of constant and homogeneous material parameters, considerable error may be incurred in evaluating *in situ* parameters without consideration of the layering effect.
2. The hydraulic visibility of features ahead of the penetrometer appears limited to the range of penetration rates given by $U_D R_D \leq 10^0$. For a standard cone advancing at 2 cm/s with a pressure-monitoring location within 1 radius of the dislocation (tip), any feature will be invisible for a coefficient of consolidation, $c \geq 1{\cdot}78$ cm^2/s. Thus, features present in a broad variety of sands, silts and clays should be readily apparent as they are approached, thus heightening the possibility of spurious parameter determination within layers as suggested (in 1) above. Where the monitoring location is more distant, the threshold magnitude of c is increased and a broader variety of soil types will exhibit visible boundaries.

3. The prior length of visibility for $U_D R_D \leq 10^0$ is not significantly influenced by the dimensionless penetration rate parameter $U_D R_D$, suggesting an invariance under a broad range of coefficient of consolidation magnitudes. As $U_D R_D$ decreases, the change in pore pressure elicited by the approached boundary becomes increasingly more apparent. The visibility length is of the order $w_D/R_D \leq 2$ suggesting that, for shaft-mounted monitors, the presence of layering is apparent at a separation ahead of the tip equal to the lag of the monitoring location behind the tip. Thus, hydraulic boundaries are theoretically more visible to monitoring locations remote from the tip when pore pressures are dissipation-controlled, as opposed to the tip when pore-pressure generation dominates. This useful artifact is of reduced significance since absolute pressure magnitudes are inversely proportional to lag behind the tip as $P_D \propto 1/R_D$, and hence, instrument sensitivity becomes of concern.
4. A similar detection length $w_D/R_D \leq 2$ applies to the tip as to shaft pressures. For standard penetration, the detection limit is of the order of 1·5 cm ahead of the tip.
5. For arrest close to a hydraulic boundary, pressures generated around the tip are controlled primarily by the material parameters $U_D \bar{R}_D$ and the proximity of the dislocation as measured through $w'_D/\bar{R}_D$. Initial steady pressure magnitudes conform to those predicted under constant penetration, and dissipation rates are, surprisingly, little influenced by the presence of boundaries. Parameter determination techniques based on dissipation rates remain therefore relatively unprejudiced by the influence of boundaries and allow layer parameters to be correctly determined. Conversely, parameter estimation methods employing peak-pressure magnitudes are subject to the greatest potential risk

ACKNOWLEDGEMENTS

The support of the Waterloo Centre for Groundwater Research, NSERC and the U.S. National Science Foundation is gratefully acknowledged.

NOTATION

a_1, a_2	dimensionless coefficient (equation (18))
b, b_D	thickness of penetrated layer, dimensionless layer thickness
c	coefficient of consolidation
i, j, l, m	indices ($\pm$ 1) generalizing series expansions for all boundary conditions
k	permeability
n	integer (1, 2) representing particular image source
p, p^s	total fluid pressure, static or initial fluid pressure
P_D	dimensionless fluid pressure
r	radius of penetrometer
R, R_D	radius to point of interest, dimensionless radius to point of interest
R'_{D_i}, R''_{D_i}	dimensionless radius relative to image dislocations pre-arrest, post-arrest
$\bar{R}_D$	dimensionless radius to point of interest from arrested tip location
S, S_D	height of penetrometer tip above lower boundary, dimensionless height
t, t', t_D	time, time to penetrometer arrest, dimensionless time
U, U_D	Penetration rate or velocity, dimensionless penetration rate
V	dislocation volume
w, w'	height of penetrometer tip above lower boundary, arrested height

w_D, w'_D	dimensionless height of penetrometer tip above lower boundary and dimensionless arrested height
x, y, z	co-ordinates relative to primary moving dislocation or penetrometer tip
x_D, y_D, z_D	dimensionless co-ordinates relative to primary moving dislocation
$x'_{D_i}, y'_{D_i}, z'_{D_i}$	dimensionless co-ordinates relative to image dislocations (equation (11) and (12))
$x''_{D_i}, y''_{D_i}, z''_{D_i}$	dimensionless co-ordinates relative to image dislocations post arrest (equation (14))
η	Dummy variable of integration
μ	fluid dynamic viscosity
ξ	diffusion parameter
τ	discrete parameter of time integration

REFERENCES

1. N. Janbu and K. Senneset, 'Effective stress interpretation of *in situ* static penetration tests,' *Proc. European Symp. on Penetration Testing, I*, Stockholm, 1974, pp. 115–120.
2. B. A. Torstensson, 'Pore pressure sounding instrument,' *Proc. ASCE Speciality Conf. on In Situ Measurement in Soil Properties, Vol.* 2, ASCE, New York, 1975, pp. 48–54.
3. G. A. Jones and D. J. A. Van Zyl, 'The piezometer probe—a useful investigation tool'. *Proc. 10th Int. Conf. on Soil Mech. and Found. Engrg., Vol.* 2 (ICSMFE), Stockholm 1981, pp. 489–496.
4. M. Battaglio, M. Jamidkowki, R. Lancellotta and M. Maniscalco, 'Piezometer probe test in cohesive deposits.' *Proc. Symp. on Cone Penetration Testing and Experience*, ASCE, New York, 1981, pp. 264–302.
5. B. Ladanyi, (1963). 'Expansion of a cavity in a saturated clay medium.' *J. Soil Mech. Found. Div.*, ASCE, **89** (4), 127–161 (1963).
6. M. M. Baligh, 'Strain path method', *J. Geotech. Eng. Div.* ASCE, **111** (9), 1108–1136 (1985).
7. A. W. Skempton, 'The pore-pressure coefficients A and B', *Geotechnique*, **4**, 143–147 (1954).
8. M. A. Biot and D. G. Willis, 'The elastic coefficient of the theory of co nsolidation', *J. Appl. Mech.* ASME, **24**, 594–601 (1957).
9. M. A. Biot, 'General theory of three-dimensional consolidation', *J. Appl. Phys.*, **12**, 155–164 (1941).
10. J. A. Geertsma, 'Remark on the analogy between thermo-elasticity and the elasticity of saturated porous media', *J. Mech. Phys. Solids*, **6**, 13–16.
11. M. P. Cleary, 'Fundamental solutions for a fluid-saturated porous solid', *Int. J. Solids Struct.*, **13** (9), 785–806 (1977).
12. D. Elsworth 'Dislocation analysis of penetration in saturated porous media', *J. Eng. Mech. Div.*, ASCE, **117** (2), 391–408 (1991a).
13. D. Elsworth 'Analysis of piezocone data using dislocation based methods', (1991b) (submitted for publication).
14. R. C. Gupta and J. L. Davison, 'Piezoprobe determined coefficient of consolidation', *Soils and Found.*, **26** (3), 12–22 (1986).
15. D. Elsworth and B. Voight, 'Poroelastic response around an intruding dike', *J. Geophys. Res.* (1991) (submitted for publication).